Neutron resonance spectroscopy of ^{106}Pd and ^{108}Pd from 20 to 2000 eV

B. E. Crawford,[1,*] J. D. Bowman,[2] P. P. J. Delheij,[3] T. Haseyama,[4] J. N. Knudson,[2] L. Y. Lowie,[5,†] A. Masaike,[4]
Y. Matsuda,[4] G. E. Mitchell,[5] S. I. Penttilä,[2] H. Postma,[6] N. R. Roberson,[1] S. J. Seestrom,[2] E. I. Sharapov,[7]
S. L. Stephenson,[5,‡] and V. W. Yuan[2]

[1]*Duke University, Durham, North Carolina 27708*
and Triangle Universities Nuclear Laboratory, Durham, North Carolina 27708-0308
[2]*Los Alamos National Laboratory, Los Alamos, New Mexico 87545*
[3]*TRIUMF, Vancouver, British Columbia, Canada V6T 2A3*
[4]*Physics Department, Kyoto University, Kyoto 606-01, Japan*
[5]*North Carolina State University, Raleigh, North Carolina 27695-8202*
and Triangle Universities Nuclear Laboratory, Durham, North Carolina 27708-0308
[6]*University of Technology, Delft, 2600 GA, The Netherlands*
[7]*Joint Institute for Nuclear Research, 141980 Dubna, Russia*
(Received 23 January 1998)

Parity nonconserving asymmetries have been measured in p-wave resonances of ^{106}Pd and ^{108}Pd. The data analysis requires knowledge of the neutron resonance parameters. Transmission and capture γ-ray yields were measured for $E_n = 20$–2000 eV with the time-of-flight method at the Los Alamos Neutron Science Center (LANSCE). A total of 28 resonances in ^{106}Pd and 32 resonances in ^{108}Pd were studied. The resonance parameters for ^{106}Pd are new for all except one resonance. In ^{108}Pd six new resonances were observed and the precision improved for many of the resonance parameters. A Bayesian analysis was used to assign orbital angular momentum for the resonances studied. [S0556-2813(98)01208-4]

PACS number(s): 24.30.$-$v, 25.40.Ny, 27.60.+j, 24.80.+y

I. INTRODUCTION

After the discovery of large parity-nonconserving enhancements in the compound nucleus by Alfimenkov *et al.* at Dubna [1], a program was initiated by the TRIPLE (time reversal invariance and parity at low energies) Collaboration to use the pulsed polarized neutron beam available at the Los Alamos Neutron Science Center (LANSCE) to study parity nonconservation in multiple resonances in many nuclei [2,3]. The analysis approach adopted assumes that the compound nucleus can be treated statistically and that from the observation of several parity nonconserving (PNC) effects, a root-mean-square (rms) PNC matrix element can be determined for each nucleus. The PNC effects manifest themselves as parity-odd asymmetries in the p-wave resonance cross section through the mixing of s-wave and p-wave resonances. Longitudinally polarized epithermal neutrons are used to measure these asymmetries for p-wave resonances in the energy range of 0.5 eV–2 keV. In an effort to measure the strength of the weak component of the effective nucleon-nucleus interaction as a function of nuclear mass, measurements in several nuclei have been studied [4–12]. The focus has been in the mass 110 and mass 230 regions where the p-wave neutron strength function peaks. Although odd mass

targets typically have about twice the level density of the even mass targets, and therefore increase the likelihood of observing PNC effects, the determination of the PNC matrix element is complicated by the fact that the s- and p-wave resonances have multiple spin possibilities. Without complete spectroscopic information, substantial uncertainty can result in the value obtained for the PNC matrix element [13,14]. For this reason and because they were available in isotopically pure form, targets of ^{106}Pd and ^{108}Pd were used to measure the longitudinal asymmetry in the total neutron capture cross section [10]. The results of these PNC measurements will be discussed in a forthcoming paper.

Measurement of the asymmetries with the isotopically pure targets were performed with a newly commissioned capture γ-ray detector [15,16]. In addition, the transmission and capture γ-ray yields were measured for these targets in order that resonance parameters could be determined. Although most of the resonance parameters are known for ^{108}Pd [17], the parameters for only one resonance below 2 keV have been published for ^{106}Pd [17]. The neutron resonance parameters are essential to determine the rms PNC matrix element. The transmission experiments were performed to obtain resonance parameters needed for the normalization of the capture data, as described in Sec. III C. The capture data were more sensitive to the weak resonances, some of which were not observed in the transmission data. Altogether a total of 28 resonances in ^{106}Pd and 32 resonances in ^{108}Pd were studied.

This paper describes these cross section measurements and the determination of the neutron resonance parameters—resonance energies, neutron widths, and radiative widths. In addition, a Bayesian analysis was performed in order to make an orbital angular momentum assignment for each

---

*Present address: North Carolina State University, Raleigh, North Carolina 27695-8202 and Gettysburg College, Gettysburg, Pennsylvania 17325.

†Present address: McKinsey and Company, Atlanta, Georgia 30303.

‡Present address: Gettysburg College, Gettysburg, Pennsylvania 17325.

resonance studied. We describe our experimental apparatus and methods in Sec. II. The analysis procedures and results are presented in Sec. III. A summary is given in Sec. IV.

II. EXPERIMENTAL APPARATUS

These experiments utilized one of the high flux, epithermal neutron beams provided at the Manuel Lujan Neutron Scattering Center (MLNSC). An 800-MeV pulsed proton beam from the LANSCE linear accelerator is bunched and shaped with a proton storage ring to form a proton beam pulsed at 20 Hz with an average beam current of about 70 μA. The proton beam has the shape of an isosceles triangle with a base of 250 ns. The proton beam is directed onto a tungsten target where the interaction of the high-energy protons with tungsten produce neutrons through the spallation process. The neutrons are then moderated to epithermal energies by a water moderator. Details of the neutron facility are discussed by Lisowski *et al.* [18].

The measurements described here were performed on flight path 2 of the MLNSC. An overview of the TRIPLE experimental apparatus is given by Roberson *et al.* [19]. The following discussion includes only those parts of the TRIPLE beam line relevant to the cross section measurements.

The neutron flux was monitored by ^{3}He and ^{4}He ionization chambers at the beginning of the beam line. Since both chambers are sensitive to γ rays, but only the ^{3}He chamber is sensitive to neutrons, subtraction of the signals from the two ionization chambers yields a measure of the incoming neutron flux. This flux measurement is not used as an absolute measurement of the flux, but rather as a sensitive measure of the beam stability.

In the transmission measurements the targets were placed at 10 m and the neutrons were detected by a ^{10}B-loaded liquid scintillator located in a counting house at 60 m. This detector is segmented into a 55-element array and viewed by 55 photomultiplier tubes [20]. The individual detector signals were filtered by 5-ns passive filters and then fed to fast discriminators with output pulse widths of 5 ns. The outputs of all 55 discriminators were linearly summed and fed to a 100-ns passive filter. This signal was then digitized by a transient digitizer.

For the capture experiments the targets were placed at the center of the capture detector, which was housed in the 60-m counting house. The capture detector consists of 24 wedge-shaped CsI crystals forming two annular rings of 12 crystals each surrounding the 4-inch diameter graphite beam pipes. Graphite was used to limit the amount of neutron scattering which can cause background. In addition, a 5-cm thick annulus of ^{6}Li-loaded polyethylene (10% ^{6}Li by weight) was inserted between the graphite pipe/target assembly and the detector. Monte Carlo calculations indicate that for neutrons below 1000 eV less than 0.15% of the scattered neutrons are transmitted through this shielding [15]. The upstream and downstream halves of the detector were combined in pairs, so that electronically the capture detector consisted of one 12-detector ring. The 12 individual detector signals were filtered by 30-ns passive filters, and to limit effects of time jitter, the signals were discriminated by constant fraction discriminators. The discrimination threshold corresponded to a

γ-ray energy of 0.3 MeV. The 12 discriminator outputs were linearly summed.

The peak height of the summed signal corresponds to the number of γ rays striking the detectors at the same time. By adjusting the threshold of a final discriminator, the summed signal was then discriminated such that only instances of two or more detectors in coincidence were counted. Experimentally this mode of operation gave the best signal-to-noise ratio with the highest count rate. Single γ rays which Compton scatter or produce electron-positron pairs and which deposit more than 0.3 MeV in two or more detectors are also recorded. The fraction of such events is determined by the discriminator thresholds and by the geometry of the detectors, and is therefore constant. This was verified by measuring the ratio of data taken with no γ-ray coincidence to that of twofold γ-ray coincidence as a function of neutron energy [16]. No energy dependence was observed. As in the transmission experiment, this signal was filtered by a 100-ns filter and then digitized by a transient digitizer. The detector design and shielding considerations are discussed by Frankle *et al.* [15]. A discussion of detector performance is given by Crawford *et al.* [16].

The processed current pulses from both the transmission and capture detectors were digitized by an 11-bit transient digitizer into 8192 channels each having a width of 100 ns. The start time for the transient digitizer was given by an inductive pick up through which the proton beam passed just before striking the tungsten spallation target. The neutron time-of-flight spectrum was determined for a time range of $\sim$8 ms which corresponds to energies down to about 20 eV. The combination of the flight-path length and the beam response produced insufficient resolution to permit analysis of resonances above about 2 keV.

The ^{106}Pd and ^{108}Pd targets were metal powders held in the shape of 3.5-inch diameter disks by aluminum cans with 20-mil thick front and back faces. The ^{106}Pd target weighed 23.3279 g and was enriched to 98.51%, giving an areal density of $n = 2.11 \times 10^{21}$ atoms/cm^2. The ^{108}Pd target weighed 21.6691 g and was enriched to 98.59%, giving an areal density of $n = 1.92 \times 10^{21}$ atoms/cm^2.

X-ray photographs of the ^{106}Pd target showed that because the metal powder had a nonuniform grain size, the ^{106}Pd target had an uneven density. This situation did not affect the analysis of the capture measurements since the experiment was sensitive to the average target thickness, and the entire target was illuminated by the beam. In the transmission measurements, however, due to tight collimation, only a small fraction of the target was illuminated. In addition, the targets were placed at 60° relative to the beam line in order to double the effective target thickness. The effective areal density of the ^{106}Pd target at 60° relative to the beam direction in transmission was measured by fitting the 281.1-eV s-wave resonance using the fitting code FITXS (described below). This resonance has a known neutron width. Because of the high statistics of these measurements, the quality of the fit was very sensitive to the target thickness. Both the neutron width and the target thickness parameters were allowed to vary in order to minimize the χ^2 of the fit. This yielded $g\Gamma_n = (519 \pm 38)$ meV as compared with the known value of $g\Gamma_n = (529 \pm 25)$ meV [17] and an areal density $n = (5.5 \pm 0.4) \times 10^{21}$ atoms/cm^2.
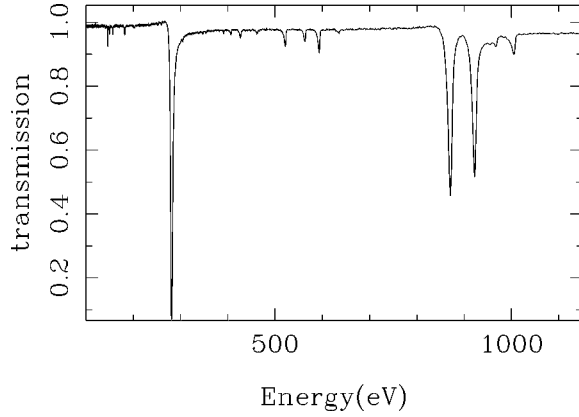
FIG. 1. Transmission spectrum of ^{106}Pd for neutron energies from 100 to 1150 eV.

X-ray photographs of the ^{108}Pd target showed a uniform target thickness throughout the entire target. By comparing the transmission areas of weak resonances when the target was placed at 0° and 60° with respect to the beam direction, the ratio of the target thicknesses for these two situations was found. For a thin target where $n\sigma \ll 1$, the transmission area is given by [21]

$$A = \frac{\pi}{2} n\sigma\Gamma, \qquad (1)$$

and therefore the ratio of the resonance areas gives the ratio of the areal densities, which was measured to be 2.1 ± 0.1. The effective areal density of the ^{108}Pd target when at 60° relative to the beam direction was found by multiplying the areal density quoted earlier by 2.1, which gives $n = 4.0 \pm 0.2$ atoms/cm^2.

The main contaminant resonances observed in the data were from ^{105}Pd: (1.01 ± 0.02)% in ^{106}Pd and (0.29 ± 0.02)% in ^{108}Pd. These values were found by averaging the fits of several resonances throughout the spectrum where the resonance parameters were held fixed to known values, and the contamination percentage was allowed to vary. In the transmission data there were also many resonances from the 0.8-mm sheet of natural Cd placed at the front of the beam line to absorb low-energy neutrons that could reach the detector after the following beam burst. Figures 1 and 2 show
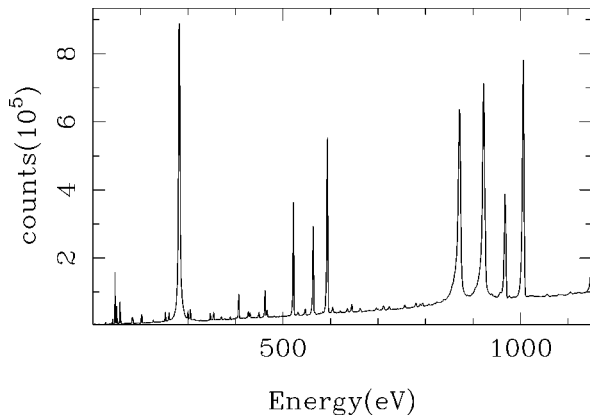
representative spectra from the transmission and capture measurements, respectively.

III. ANALYSIS

A. Fitting code

In order to extract resonance parameters, the data from both capture and transmission experiments were fit with the fitting code FITXS [11], which was developed specifically to fit the time-of-flight spectra measured by the TRIPLE Collaboration. One chooses a particular time-of-flight region and a set of fitting parameters and then minimizes χ^2 to obtain the optimum set of values for these parameters. The fitting function depends on the target areal density, the multilevel cross sections, and broadening due to three sources: the time structure of the neutron beam, the Doppler broadening due to the relative motion between neutrons and target nuclei, and the time response of the detection system. The broadening due to the beam and the detection system can be combined analytically to form a response function $B(t)$.

For the transmission experiment, the fitting function can be written as

$$\mathcal{F}_t(t) = B_t(t) \otimes [N_0(t)e^{-n\sigma_D(t)}] + \mathcal{B}_t, \qquad (2)$$

and for the capture experiment the fitting function can be written as

$$\mathcal{F}_c(t) = B_c(t) \otimes \left[N_0(t)\frac{\sigma_{\gamma D}}{\sigma_D}(1 - e^{-n\sigma_D(t)}) \right] + \mathcal{B}_c, \qquad (3)$$

where

$$\sigma_{\gamma D}(t) = [D(v) \otimes \sigma_\gamma(v)]_{v \to t} \quad \text{and}$$

$$\sigma_D(t) = [D(v) \otimes \sigma(v)]_{v \to t}, \qquad (4)$$

N_0 is the neutron flux, $D(v)$ is the Doppler response function, $\mathcal{B}_t$ and $\mathcal{B}_c$ are the background functions, and the $v \to t$ symbol indicates that after the convolution in velocity space, the function is converted to a function of time. The symbol $\otimes$ indicates a convolution.

The multilevel, multichannel neutron cross section is calculated with the formalism of Reich and Moore [22], which is widely used in the analysis of neutron resonances [23]. For ^{106}Pd and ^{108}Pd there is no fission and the ratio of the total resonance width Γ to the level spacing D is small ($\Gamma/D \sim 0.005$). The s-wave elastic cross section for total angular momentum J is

$$\sigma^{el}_{s:J} = \pi \lambda^2 g_J \left| 1 - e^{-2ikR}\left[1 + \frac{2if_J}{1 - if_J} \right] \right|^2, \qquad (5)$$

with

$$f_J = \sum_{s:J} \frac{\Gamma^s_n/2}{E_s - E - i\Gamma^s_\gamma/2}, \qquad (6)$$

where $g_J = (2J+1)/2$ is the statistical weighting factor for $I = 0$, λ is the neutron wave length divided by 2π, and R is the neutron channel radius. The experimentally determined

FIG. 2. Capture yield spectrum for ^{106}Pd for neutron energies from 100 to 1150 eV.
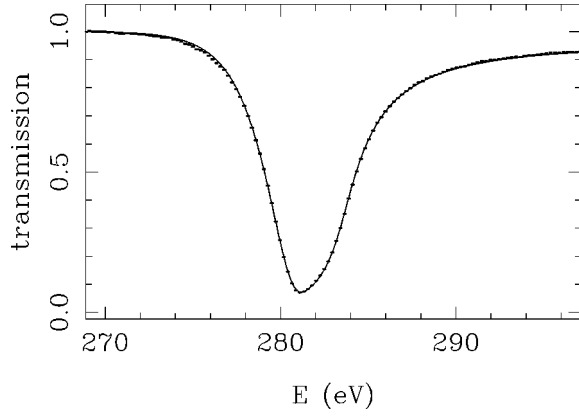
FIG. 3. Transmission for the 281.1-eV *s*-wave resonance in ^{106}Pd. The solid line is a fit to the data as described in the text.

potential scattering radius [17] is used for R. The resonance energy is $E_{s,p}$; the neutron width is $\Gamma_n^{s,p}$; the γ-ray width is $\Gamma_\gamma^{s,p}$; and the total width is $\Gamma^{s,p}$, for *s*- and *p*-wave resonances, respectively. The *s*-wave capture cross section is

$$\sigma_{s:J}^\gamma = 4\pi\lambdabar^2 g_J \frac{\mathrm{Im}\{f_J\}}{[1+\mathrm{Im}\{f_J\}]^2 + \mathrm{Re}\{f_J\}^2}. \tag{7}$$

With $\Gamma_n \ll \Gamma_\gamma \ll D$ and the *p*-wave hard-sphere phase shift neglected [24], the *p*-wave elastic cross section is

$$\sigma_{p:J}^{\mathrm{el}} = \pi\lambdabar^2 g_J \sum_{p:J} \frac{\Gamma_n^p \Gamma_n^p}{(E_p - E)^2 + (\Gamma^p)^2/4}. \tag{8}$$

For the *p*-wave capture cross section similar simplifications [22] yield

$$\sigma_{p:J}^\gamma = \pi\lambdabar^2 g_J \sum_{p:J} \frac{\Gamma_n^p \Gamma_\gamma^p}{(E_p - E)^2 + (\Gamma^p)^2/4}. \tag{9}$$

The neutron widths are calculated at energy E according to

$$\Gamma_n^{s,p}(E) = \Gamma_n^{s,p}(E_{s,p})[E/E_{s,p}]^{l+1/2}. \tag{10}$$

The total cross section for both *s*- and *p*-wave resonances is simply the sum of the elastic and capture cross sections.

TABLE I. Resonance parameters for ^{106}Pd.

E (eV)	Transmission $g\Gamma_n$ (meV)	Capture $g\Gamma_n$ (meV)	Γ_γ (meV)	B.P. [a]	l [b]	Source [c]
63.43±0.04	0.012±0.001	0.010±0.001	107±12	0.99	1	c
146.36±0.07	0.54±0.05	0.53±0.04	97±7	0.97	1	c
156.88±0.07	0.26±0.03	0.24±0.02	107±8	0.98	1	c
281.1±0.3	519±52			0.00	0	t
300.0±0.2		0.18±0.02		0.98	1	c
406.7±0.3	0.78±0.08	0.86±0.04		0.97	1	c
462.3±0.3	1.20±0.12	1.14±0.05		0.97	1	c
521.9±0.4	6.7±0.7	6.0±0.3		0.89	1	c
563.4±0.5	5.4±0.5	5.3±0.3		0.91	1	c
593.4±0.5	12±1	12.5±0.6		0.72	0(?)	c
644.9±0.6		0.52±0.05		0.97	1	c
871±1	925±93			0.00	0	t
922±1	745±75			0.00	0	t
967.5±0.6	15±2	16±1		0.84	1	c
1005.3±0.7	38±4	58±4		0.10	0	c
1147.9±0.9	3±1	4.0±0.4		0.95	1	c
1206.2±0.9	7.6±0.8	10.0±0.7		0.92	1	c
1306±1		3.4±0.3		0.95	1	c
1323±1		7.8±0.8		0.93	1	c
1377±1		2.2±0.2		0.95	1	c
1398±2	231±23			0.00	0	t
1511±2	18±2	28±2		0.84	1	c
1557±2		1.7±0.2		0.95	1	c
1585±3	158±16			0.02	0	t
1597±2		12±1		0.92	1	c
1624±2		10±1		0.93	1	c
1764±2	15±3	18±2		0.91	1	c
1839±4	914±92			0.00	0	t

[a]Bayesian *p*-wave probability.
[b]Orbital angular momentum assignments are from the Bayesian analysis.
[c]For the Bayesian analysis, resonance parameters are from: c-capture and t-transmission. All resonances except the one at 281.1 eV are new resonances.

TABLE II. Resonance parameters for ^{108}Pd.

| | Transmission | Capture | | Ref. [17] | | | |
E (eV)	$g\Gamma_n$ (meV)	$g\Gamma_n$ (meV)	Γ_γ (meV)	$g\Gamma_n$ (meV)	B.P. [a]	l [b]	Source [c]
33.02±0.05	115±12			117±8	0.00	0	t
90.9±0.1	210±21			199±8	0.00	0	t
112.70±0.07	1.0±0.1	0.96±0.08	114±10	2.3±0.3	0.85	1	c
149.76±0.07	0.036±0.009	0.060±0.006		0.16±0.02	0.99	1	c
302.9±0.2	3.6±0.4	3.2±0.2	102±5	3.91±0.04	0.87	1	c
411.0±0.3	0.55±0.06	0.65±0.03		0.80±0.04	0.98	1	c
426.9±0.3	390±39			402.5±4.1	0.00	0	t
480.5±0.4	0.7±0.1	0.57±0.03		0.61±0.05	0.98	1	c
544.4±0.4	4.7±0.5	5.6±0.3		5.90±0.08	0.90	1	c
635.3±0.6	433±43			462.1±6.4	0.00	0	t
642.2±0.6		1.3±0.1		2.13±0.07	0.97	1	c
797.4±0.8	6.1±0.6	6.3±0.4		7.17±0.12	0.93	1	c
843.4±0.9		0.83±0.08		1.55±0.11	0.97	1	c
905±1	594±59			581±12	0.00	0	t
956±1	888±88			1018±15	0.00	0	t
962.40±0.96				47.1±0.4	0.10	0	m
1082.3±0.8	21±2	17±1		11±5	0.85	1	c
[d]1121±2		0.51±0.05			0.97	1	c
[d]1140±2		0.08±0.02			0.97	1	c
1215±2	418±42			418±13	0.00	0	t
1359±1	27±3	28±2		24±5	0.79	1(?)	c
1433±2	148±15			139±7	0.00	0	t
1456±1		4.5±0.5		5.0±1.5	0.95	1	c
[d]1505±2		0.33±0.05			0.96	1	c
1523±2		2.8±0.3		2.0±1.7	0.96	1	c
1652±3	1269±127			1558±23	0.00	0	t
1710±3	77±8			76.5±9.0	0.34	0	t
[d]1743±2		0.47±0.07			0.96	1	c
[d]1815±2		2.4±0.2			0.96	1	c
2008±2				10±3	0.94	1	m
2008±4	696±70			813±23	0.00	0	t
2118±3		7.5±0.8		8±3	0.95	1	c
[d]2165±3		2.6±0.3			0.95	1	c
2287±4		37±4		50±7	0.87	1	c

[a]Bayesian p-wave probability.
[b]Orbital angular momentum assignments are from the Bayesian analysis.
[c]For the Bayesian analysis, resonance parameters are from: c-capture, t-transmission, or m-Ref. [17].
[d]New resonances.

Initial investigations into the resolution function were performed by Yen et al. [25] The authors obtained fits to Monte Carlo simulations of the beam time response for the TRIPLE beam line using a function formed from convoluting a Gaussian with an exponential tail. Their results were extended by fitting resonance data obtained with the capture detector. Since above about 400 eV most of the observed width is due to the experimental response, fits of the capture data were sensitive to the response parameters, especially the exponential tail. We found that to obtain satisfactory fits, a second exponential tail was required, giving the functional form

$$B_c(t) = \frac{1}{2\tau} \exp\left[\frac{-(t-t_0)}{\tau} + \frac{\kappa^2}{2\tau^2}\right][1 - \mathrm{erf}(Z)]$$
$$+ \frac{\epsilon}{2\tau_2} \exp\left[\frac{-(t-t_0)}{\tau_2} + \frac{\kappa^2}{2\tau_2^2}\right][1 - \mathrm{erf}(Z_2)],$$

(11)

where $Z_2 = [\kappa/\tau_2 - (t-t_0)/\kappa]/\sqrt{2}$. The Gaussian width, κ, includes broadening from three sources modeled as Gaussians and whose widths are added in quadrature: the neutron
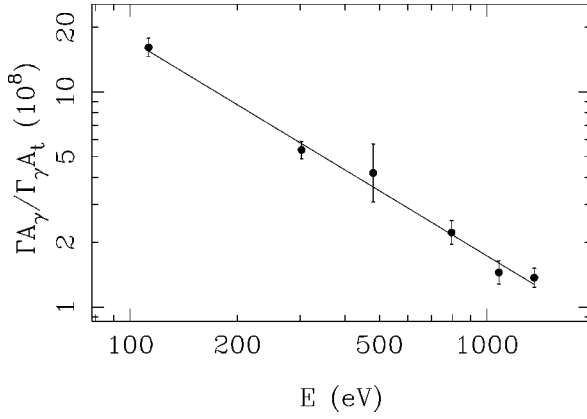
FIG. 4. Determination of the energy dependence of the neutron flux times the capture detector efficiency.

moderator ($0.65E^{-0.51}$ μs), electronic signal filtering (43 ns), and the proton beam (52 ns). The time offset is $t_0 = 2.79E^{-0.48}$ μs, and the first exponential tail has characteristic decay time, $\tau = 0.99E^{-0.37}$ μs. These parameters were determined by Yen *et al.* and were held constant while resonances in ^{106,108}Pd were fit. We found $\epsilon = 0.20$, and $\tau_2 = 3.9E^{-0.38}$ μs.

The transmission data showed an additional broadening from the neutron detector. The moderation process in the ^{10}B detector is given by an exponential with characteristic decay time τ_d. The final result for the response function is

$$B_t(t) = \frac{1}{2(\tau - \tau_d)} \{ e^{-(t-t_0)/\tau_d + \kappa^2/2\tau_d^2} [1 - \mathrm{erf}(Z_d)]$$

$$- e^{-(t-t_0)/\tau + \kappa^2/2\tau^2} [1 - \mathrm{erf}(Z)] \}$$

$$+ \frac{\epsilon}{2(\tau_2 - \tau_d)} \{ e^{-(t-t_0)/\tau_d + \kappa^2/2\tau_d^2} [1 - \mathrm{erf}(Z_d)]$$

$$- e^{-(t-t_0)/\tau_2 + \kappa^2/2\tau_2^2} [1 - \mathrm{erf}(Z_2)] \}, \quad (12)$$

where $Z = [\kappa/\tau - (t-t_0)/\kappa]/\sqrt{2}$, $Z_d = [\kappa/\tau_d - (t-t_0)/\kappa]/\sqrt{2}$, and $Z_2 = [\kappa/\tau_2 - (t-t_0)/\kappa]/\sqrt{2}$. The average value of
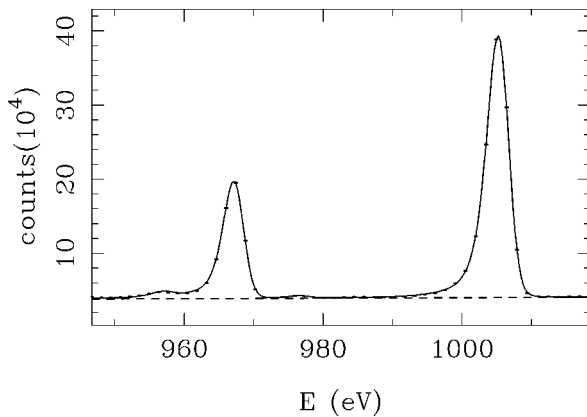

FIG. 5. Data and fit of the capture yield of the 967.5 and 1005.3-eV resonances in ^{106}Pd. The small peaks are from the 956-eV *s*-wave resonance in ^{108}Pd and the 976.7-eV *s*-wave resonance in ^{105}Pd.
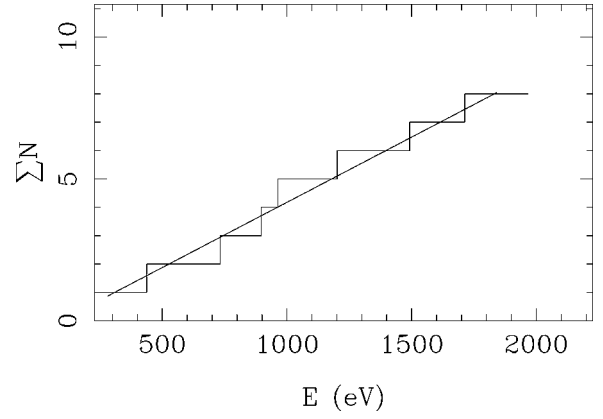

FIG. 6. Cumulative number of levels for ^{106}Pd *s*-wave resonances with a linear fit used to extract the *s*-wave level spacing.

$\tau_d = 416$ ns was determined from fitting nine resonances in ^{108}Pd. The details are given by Crawford [10].

Including an energy-dependent flux and allowing for background (described by a polynomial in time), the final fitting functions can be written as

$$\mathcal{F}_t(t) = \left[B_t(t) \otimes \left[\frac{\alpha}{E^\beta} e^{-n\sigma_D(t)} \right] \right] + \sum_{i=0}^{3} \frac{a_i}{t^i} \quad (13)$$

for the transmission experiment, and

$$\mathcal{F}_c(t) = \left[B_c(t) \otimes \left[\frac{\alpha}{E^\beta} \frac{\sigma_{\gamma D}}{\sigma_D} (1 - e^{-n\sigma_D(t)}) \right] \right] + \sum_{i=0}^{3} b_i t^i \quad (14)$$

for the capture experiment, where $\sigma_D(t)$ is the Doppler-broadened total cross section, and $\sigma_{\gamma D}(t)$ is the Doppler-broadened capture cross section for *s*- and *p*-wave resonances. The *s*- and *p*-wave cross sections are calculated for all resonances present (including contaminants) and summed to form the total elastic and capture cross sections.

B. Transmission

In order to calibrate the neutron time of flight to neutron energy, the peak channels of 39 known Cd resonances were determined and a least-squares fit of the channel versus en-
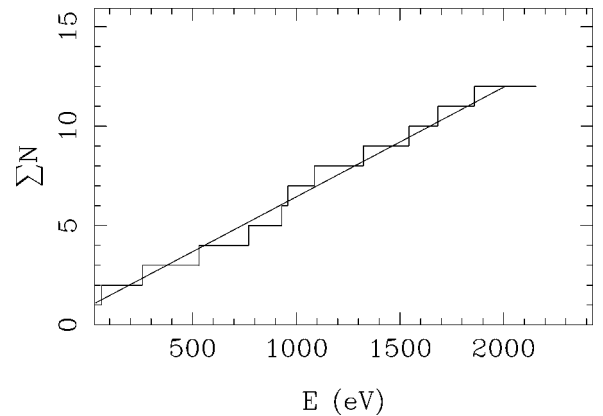

FIG. 7. Cumulative number of levels for ^{108}Pd *s*-wave resonances with a linear fit used to extract the *s*-wave level spacing.

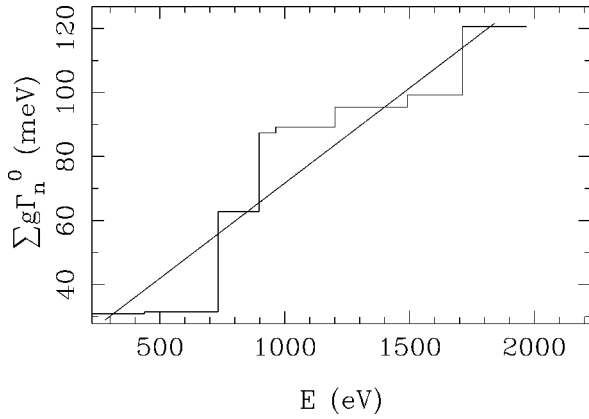FIG. 8. Cumulative reduced neutron width for [106]Pd *s*-wave resonances with a linear fit used to extract the *s*-wave strength function.

FIG. 10. Cumulative number of levels for [106]Pd *p*-wave resonances with a linear fit of resonances below 1000 eV used to extract the *p*-wave level spacing.

ergy was used to extract the beam line length, (56.802 ± 0.044) m, and the channel offset, (38.4 ± 1.4) channels. The uncertainty in these values dominates the uncertainty in the resonance energies, since statistical uncertainties are less than 0.05%. The data were next corrected for background [26] and dead time [10]. A transmission spectrum was formed (see Fig. 1) by dividing the spectrum measured when the target was in the beam by the spectrum obtained when the target was out of the beam. These transmission spectra were then fit with the fitting code FITXS described in the preceding section.

Because the level density of these even mass targets is small, almost all of the resonances were well separated. A sample fit is given in Fig. 3. Tables I and II list the resonance energies and neutron widths for [106]Pd and [108]Pd, respectively.

Since in transmission none of these resonances showed sensitivity to the radiative width, it was held constant at 91 meV, the average of the radiative widths listed in [17] for [108]Pd. The uncertainties given for the energy values were determined from the uncertainties in the beam line length and channel offset. The uncertainties given for the neutron widths include the statistical uncertainty, the uncertainty in the effective areal density of the target and an estimate of the
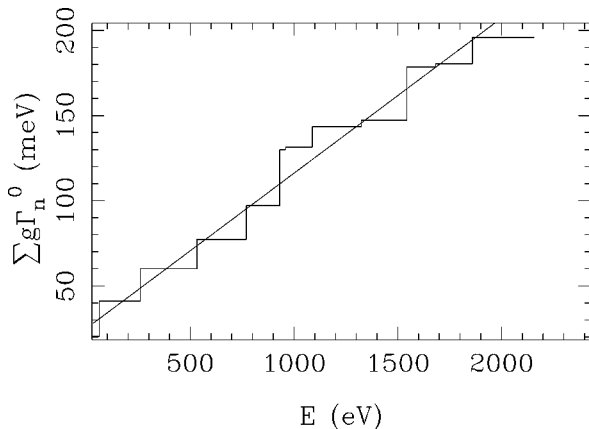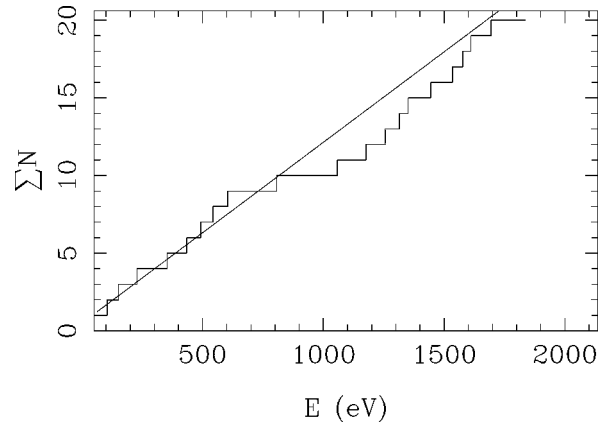
uncertainties from the fitting process. The 149.7-eV resonance in [108]Pd has an additional 4% uncertainty from the uncertainty in the width of the [105]Pd resonance at 150 eV that is unresolved from the [108]Pd resonance. Mughabghab also lists a resonance in [108]Pd at 962.4 eV which is unresolved from the 956-eV resonance seen in these data. The neutron width of 47.1 eV from Mughabghab *et al.* [17] was used for the 962.4-eV resonance when fitting the 956-eV resonance.

C. Capture

The calibration of neutron time of flight to neutron energy was obtained by identifying 49 known [105]Pd resonances in the [106]Pd spectrum and using these channels to determine the neutron energy as described above. The beam line length was (59.340 ± 0.014) m and the channel offset (508.31 ± 0.37) channels. Before resonance parameters could be extracted from the capture data, the flux and detector efficiency had to be determined. The area in a capture yield peak is given by

$$A_\gamma = \Phi(E) \epsilon \frac{\Gamma_\gamma}{\Gamma} A_t, \tag{15}$$

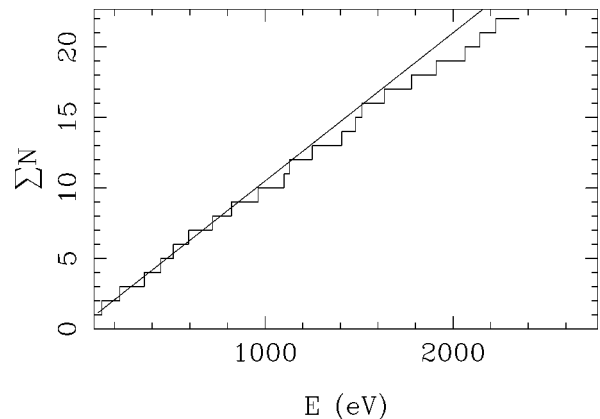where A_t is the resonance area from transmission in units of

FIG. 9. Cumulative reduced neutron width for [108]Pd *s*-wave resonances with a linear fit used to extract the *s*-wave strength function.

FIG. 11. Cumulative number of levels for [108]Pd *p*-wave resonances with a linear fit of resonances below 1000 eV used to extract the *p*-wave level spacing.
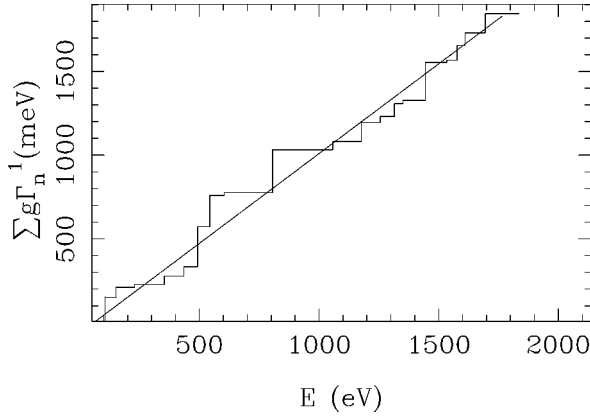
FIG. 12. Cumulative reduced neutron width for ^{106}Pd p-wave resonances with a linear fit of resonances below 1000 eV used to extract the p-wave strength function.

FIG. 13. Cumulative reduced neutron width for ^{108}Pd p-wave resonances with a linear fit of resonances below 1000 eV used to extract the p-wave strength function.

energy and normalized to 100% transmission off resonance. The energy-dependent flux $\Phi(E)$ times detector efficiency ϵ is modeled as a power law [19],

$$\Phi(E)\epsilon = \frac{\alpha}{E^{\beta}}. \tag{16}$$

By comparing the area in transmission peaks to that of capture peaks for resonances with $\Gamma_{\gamma} \sim \Gamma$, the parameters were determined: $\alpha = 6.20 \times 10^{8}$ counts-eV and $\beta = 1.00$, with the uncertainty in the resultant flux times efficiency given by

$$\frac{\Delta\Phi\epsilon}{\Phi\epsilon} = \sqrt{0.002\,01 + 0.002\,43[\ln(E) - 6.12]^{2}}. \tag{17}$$

Figure 4 shows the fit used to determine the flux times efficiency for the ^{108}Pd capture data. Since only the target was changed between the ^{106}Pd and ^{108}Pd experiments, this normalization also is used for the ^{106}Pd analysis. The error bars include the uncertainty in the thickness of the target used in transmission at 60° relative to the beam line and the uncertainty in the resonance areas from both the transmission and capture data. Effects of the uncertainty in the resonance parameters, Γ and Γ_{γ}, were negligible when compared with the other uncertainties.

We did not analyze the strong s-wave resonances which showed an asymmetric shape due to the contribution of neutron capture after multiple scattering in the sample. In such events the incoming neutrons with energies higher than the resonance energy reach the target earlier in time of flight than the resonance neutrons and lose energy by scattering within the target. They are then captured and counted as
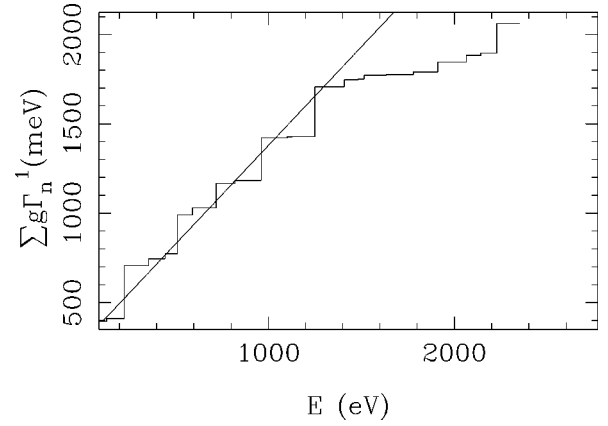
resonance neutrons. A computer code that simulates the experimental conditions using Monte Carlo techniques has been written by Stephenson *et al.* [27]. It was used for numerical estimates of multiple-scattering effects in resonances. For example, for the resonance at 33.02 eV in ^{108}Pd the capture after multiple scattering contributed 41% to the capture yield and led to a double-humped shape of the resonance curve. Since these corrections have not been included in the fitting code, FITXS, we do not extend the analysis of the capture data to such cases.

The flux parameters, α and β, were held constant as the data were fit to extract resonance parameters. The background, seen in the off resonance regions of Fig. 2, is a smoothly varying function of time of flight and was easily fit in an isolated region with a polynomial. The statistical uncertainty in determining this background was much smaller than other uncertainties that contribute to the overall uncertainties in the resonance parameters. Figure 5 shows a sample fit of capture resonances in ^{106}Pd. Since the beam timing response dominates the resonance line shape above about 400 eV, only resonances at lower energies showed sensitivity to the radiative width. The average for the 63.43, 146.36, and 156.88-eV resonances in ^{106}Pd is $\Gamma_{\gamma} = (102 \pm 5)$ meV, and the average for the 112.70 and 302.88-eV resonances in ^{108}Pd is $\Gamma_{\gamma} = (104 \pm 4)$ meV. Since only one target thickness was used and the time-of-flight resolution function dominates the line shape, the extracted value of $g\Gamma_{n}$ is very sensitive to the assumed value of Γ_{γ} for resonances where $\Gamma_{n} \gtrsim \Gamma_{\gamma}$. Therefore, reliable values of $g\Gamma_{n}$ could be determined only for resonances with $\Gamma_{n} < \Gamma_{\gamma}$. The resonance parameters obtained from the capture data are shown in Tables I and II. The uncertainties in the widths are domi-

TABLE III. S- and p-wave strength functions for ^{106}Pd and ^{108}Pd.

	^{106}Pd		^{108}Pd	
	Current [a]	Previous [b]	Current [a]	Previous [c]
S_0 (10^{-4})	0.6 ± 0.3	0.34 ± 0.04	0.9 ± 0.4	0.78 ± 0.17
S_1 (10^{-4})	4 ± 1	5.2 ± 0.5	4 ± 1	4.4 ± 0.5

[a]Values from this work (20–2000 eV).
[b]Values from Mughabghab (2–20 keV) [17].
[c]Values from Mughabghab (2–9000 eV) [17].

nated by the uncertainty in the flux times efficiency given in Eq. (17).

D. Orbital angular momentum

Following the Bayesian approach of Bollinger and Thomas [28] and using the notation of Frankle *et al.* [29], the probability of a resonance being a p wave can be related to the s-wave and p-wave neutron strength functions and hence the neutron widths:

$$P(p, g\Gamma_n)$$

$$= \left\{ 1 + \frac{\pi_s}{\pi_p} \sqrt{3 \frac{\pi_s}{\pi_p} \frac{S_1 C_0(E)}{S_0 C_1(E)}} \right.$$

$$\left. \times \exp\left[\frac{-g\Gamma_n}{2} \frac{C_0(E)}{D_0} \left(\frac{1}{S_0} - \frac{\pi_p}{3\pi_s} \frac{C_1(E)}{C_0(E)S_1} \right) \right] \right\}^{-1},$$

$$(18)$$

where π_s and π_p are the *a priori* probabilities of forming an s-wave or p-wave resonance, respectively. Assuming that these probabilities are proportional to $2J+1$, the ratio π_s/π_p is 1/3, 4/9, and $\sim 1/2$ for target spins equal to 0, 1/2, and ≥ 1, respectively. D_0 is the s-wave level spacing; D_1 is the p-wave level spacing and was assumed to equal $(\pi_s/\pi_p)D_0$ in deriving Eq. (18); $S_{0,1}$ are the s- and p-wave strength functions, respectively; and

$$C_l(E) = \frac{1 + (kR)^l}{(kR)^{2l} \sqrt{E(eV)}}. \qquad (19)$$

The strength functions are given by

$$S_l = \frac{1}{2l+1} \frac{\langle g\Gamma_n^l \rangle}{D_l}, \qquad (20)$$

where $g\Gamma_n^l$ is the reduced neutron width given by

$$g\Gamma_n^l = C_l(E)g\Gamma_n. \qquad (21)$$

Since for spin-zero targets $\pi_p = 0.75$, resonances for which Eq. (18) had $P > 0.75$ were assigned $l=1$ and resonances with $P < 0.75$ were assigned $l=0$. Because the angular momentum assignments affect the determination of the level densities and the strength functions, an iterative process of calculating probabilities, making assignments, and determining the level densities and strength functions was used until the assignments stabilized. Tables I and II list the p-wave probabilities and the orbital angular momentum assignments for ^{106}Pd and ^{108}Pd, respectively. The probabilistic procedure is not reliable when the p-wave probability is close to

the *a priori* probability. These cases have been indicated with a ''?'' in the l column in Tables I and II.

Figures 6 and 7 show the cumulative number of levels, and Figs. 8 and 9 the cumulative reduced neutron width for the s-wave resonances of ^{106}Pd and ^{108}Pd, respectively. A least-squares fit of these curves yields the s-wave level spacing and strength function for each isotope. The uncertainties for the strength functions were calculated from $\sqrt{2/N}$, where N is the number of levels analyzed [30]. Similar curves for the p-wave resonances are shown in Figs. 10–13, where only resonances below 1000 eV were used in the linear fits.

The average s-wave level spacings were found to be 217 ± 61 eV for ^{106}Pd and 182 ± 33 eV for ^{108}Pd. The ^{108}Pd value agrees qualitatively with previous measurements when evaluated in the same energy range [17]. Since only one s-wave below 2 keV was observed previously in ^{106}Pd, this comparison is not possible for ^{106}Pd. The average p-wave level spacings are 85 ± 19 eV for ^{106}Pd and 95 ± 24 eV for ^{108}Pd. The latter value differs from the expected value of $D_0/3$, possibly indicating the effect of unobserved p-wave levels. Table III lists the strength functions determined with the above method as compared with previous determinations [17]. The s- and p-wave strength functions are consistent with previous measurements.

IV. SUMMARY

Measurements of the transmission and capture γ-ray yields were performed for ^{106}Pd and ^{108}Pd in the energy range 20–2000 eV. The neutron time of flight was calibrated to neutron energy by identifying known resonances of Cd and ^{105}Pd in the spectra. This calibration was used to determine the neutron resonance energies. Using the multilevel fitting code FITXS, resonances were fit to determine $g\Gamma_n$ and Γ_γ. A total of 28 resonances in ^{106}Pd, all but one previously unreported, were observed and analyzed. Thirty-two resonances in ^{106}Pd, six of which are new, were observed and analyzed. A Bayesian analysis was used to estimate the probability of a resonance being p wave. In addition, the s- and p-wave level spacings and strength functions were determined. Knowledge of the ^{106}Pd and ^{108}Pd resonance parameters permits the extraction of the rms weak matrix elements from observed parity nonconserving asymmetries [10,12], which will be published in forthcoming papers.

[1] V. P. Alfimenkov, S. B. Borzakov, Vo Van Thuan, Yu. D. Mareev, L. B. Pikelner, A. S. Khrykin, and E. I. Sharapov, Nucl. Phys. **A398**, 93 (1983).

[2] J. D. Bowman, G. T. Garvey, Mikkel B. Johnson, and G. E. Mitchell, Annu. Rev. Nucl. Part. Sci. **43**, 829 (1993).

[3] C. M. Frankle, S. J. Seestrom, N. R. Roberson, Yu. P. Popov, and E. I. Sharapov, Phys. Part. Nuclei **24**, 401 (1993).

[4] J. D. Bowman *et al.*, Phys. Rev. Lett. **65**, 1192 (1990).

[5] X. Zhu *et al.*, Phys. Rev. C **46**, 768 (1992).

[6] C. M. Frankle *et al.*, Phys. Rev. Lett. **67**, 564 (1991).

[7] C. M. Frankle *et al.*, Phys. Rev. C **46**, 778 (1992).

[8] S. L. Stephenson, Ph.D. thesis, North Carolina State University, 1996.

[9] L. Y. Lowie, Ph.D. thesis, North Carolina State University, 1996.

[10] B. E. Crawford, Ph.D. thesis, Duke University, 1997.

[11] Y. Matsuda, Ph.D. thesis, Kyoto University, 1998.

[12] D. A. Smith *et al.* (unpublished).

[13] J. D. Bowman, L. Y. Lowie, G. E. Mitchell, E. I. Sharapov, and Yi-Fen Yen, Phys. Rev. C **53**, 285 (1996).

[14] J. D. Bowman, L. Y. Lowie, and E. I. Sharapov, Phys. Part. Nuclei **27**, 398 (1996).

[15] C. M. Frankle, J. D. Bowman, S. J. Seestrom, N. R. Roberson, and E. I. Sharapov, *Time Reversal Invariance and Parity Violation in Neutron Resonances*, edited by C. R. Gould, J. D. Bowman, and Yu. P. Popov (World Scientific, Singapore, 1994), p. 204.

[16] B. E. Crawford *et al.*, *IV International Seminar on Interactions of Neutrons with Nuclei* (JINR, Dubna, 1997), p. 268.

[17] S. F. Mughabghab, M. Divadeenam, and N. E. Holden, *Neutron Cross Sections, volume 1 part A* (Academic, New York, 1981).

[18] P. W. Lisowski, C. D. Bowman, G. J. Russell, and S. A. Wender, Nucl. Sci. Eng. **106**, 208 (1990).

[19] N. R. Roberson *et al.*, Nucl. Instrum. Methods Phys. Res. A **326**, 549 (1993).

[20] Yi-Fen Yen *et al.*, *Time Reversal Invariance and Parity Violation in Neutron Resonances* [15], p. 210.

[21] E. Melkonian, W. W. Havens, Jr., and L. J. Rainwater, Phys. Rev. **92**, 702 (1953).

[22] C. W. Reich and M. S. Moore, Phys. Rev. **111**, 929 (1958).

[23] Cross Section Evaluation Working Group, BNL-NCS-44945 (ENDF-102) (1995).

[24] J. E. Lynn, *The Theory of Neutron Resonance Reactions* (Clarendon, Oxford, 1968).

[25] Yi-Fen Yen, E. J. Pitcher, and J. D. Bowman (unpublished).

[26] Yi-Fen Yen, J. D. Bowman, L. Y. Lowie, Y. Masuda, G. E. Mitchell, and S. I. Penttilä, Nucl. Instrum. Methods Phys. Res. A **397**, 365 (1997).

[27] S. L. Stephenson *et al.*, *IV International Seminar on Interactions of Neutrons with Nuclei* [16], p. 171.

[28] L. M. Bollinger and G. E. Thomas, Phys. Rev. **171**, 1293 (1968).

[29] C. M. Frankle, E. I. Sharapov, Yu. P. Popov, J. A. Harvey, N. W. Hill, and L. W. Weston, Phys. Rev. C **50**, 2774 (1994).

[30] H. Malecki, L. B. Pikelner, I. M. Salamatin, and E. I. Sharapov, Sov. J. Nucl. Phys. **11**, 61 (1970).